

FLUTTER SUPPRESSION USING V-STACK PIEZOELECTRIC ACTUATOR

Emil V. Ardelean*, Mark A. McEver, Daniel G. Cole and Robert L. Clark

*Pratt School of Engineering
Mechanical Engineering and Materials Science Department
Duke University, Durham, NC 27708, USA*

Abstract

Aeroelastic control of wings using distributed, trailing-edge control surfaces is of interest regarding maneuvers, gust alleviation, and flutter suppression. The use of high energy density, piezoelectric materials as motors provides an appealing solution to this problem. A new piezoelectric actuator (V-Stack Piezoelectric Actuator) was designed and bench tested. This actuator meets the requirements for trailing edge flap actuation in both stroke and force. It is compact, simple, sturdy, and leverages stroke geometrically with minimum force penalties while displaying linearity over a wide range of stroke. Integration of the actuator inside a structure requires minimal modifications. The shape of the actuator makes it extremely suitable for trailing edge flap actuation eliminating the need of a push rod. It leads to smaller number of parts, less added mass, less compliance and simplicity of the actuation mechanism. The actuator transmits the stroke and force through its “tip,” which is connected to the flap through a slider attached to the flap and located close to the hinge line. A typical section prototype was constructed and tested experimentally in the wind tunnel at Duke University. This experiment was designed for preliminary evaluation of the actuation concept. Operating in closed-loop, the flutter was suppressed at the speed at which the flutter occurred open-loop, and the flutter speed was increased by 21.8%.

Nomenclature

b	- semichord	I_{fCG}	- moment of inertia of the flap
c	- chord-length	K_α	- pitch stiffness
CG	- position of the center of mass of the wing model w/r/t 1/4 chord point	K_β	- flap stiffness
e	- position of the elastic axis w/r/t half-chord point	K_h	- plunge stiffness
fCG	- position of the center of mass of the flap w/r/t 3/4 chord point	l	- length (span) of the wing model
h	- wing section plunging distance at 1/4 chord point	m	- total mass of the wing model
h_l	- position of the hinge line w/r/t half-chord point	m_f	- mass of the flap
I_{CG}	- moment of inertia of the wing model	m_{bl}	- mass of the lower mounting block
		m_{bu}	- mass of the upper mounting block (including the sensor)
		r_β	- distance between flap hinge line and flap actuation point
		s	- actuator stroke
		U	- air flow speed
		α	- wing section pitch angle about 1/4 chord

*Corresponding author: PO Box 90302, Duke University, Durham, NC 27708, USA; email: ardelean@duke.edu, Tel: +1-919-660-5375, Fax: +1-919-660-5409

- β - angular deflection of the flap
- ρ - air density

Introduction

Recent developments of new piezoceramic actuation systems have made flutter alleviation using trailing edge flaps more feasible. The latest results are encouraging in spite of the fact that the piezoelectric transduction devices are not technologically mature for large stroke applications, but they are used in numerous other applications.¹⁻⁶

The actuation of trailing edge flaps of helicopter blades and high aspect ratio wings at the frequencies required for flutter alleviation and vibration control is not a trivial matter. Actuators are required to respond quickly and to produce relatively large displacements and large forces. In general, a flap displacement of $\pm 5^\circ$ to 10° is required. At Duke University, as part of an effort to build an adaptive high aspect ratio wing, a new actuator, called V-Stack Piezoelectric Actuator was developed.⁶ Preliminary tests performed on the actuator indicated that integration of the actuator into a wing model for driving a trailing edge flap should give good results. The actuator uses two stacks of high performance piezoceramic as active elements. The stacks are symmetrically positioned with respect to a central element (lever) and work complementarily. The shape of the actuator facilitates its integration into an airfoil, re-

quiring very few additional elements. This helps to make the structure simple and efficient (mass, stiffness, construction, etc.). A typical section (NACA 0015), referred to as a wing model in the following, suitable for testing in the wind tunnel at Duke University, was constructed and tested experimentally. The primary objective of our research is to increase the flutter boundary by controlling the flap in a closed-loop fashion. Aeroelastic analysis of the wing predicted the flutter free stream velocity at 19 m/s, and a flutter frequency of 4.2 Hz. The wing was first tested on the bench and then tuned for testing in the wind tunnel. The tuning was related primarily to the actuator - flap system, due to issues addressed in the following paragraphs.

Design and construction of the experimental model

The shape of the actuator (V) triggered the idea that the actuator could be mounted in the direction of the chord. By positioning the actuator chordwise, the actuator output point could be located very close to the hinge of the flap, eliminating the need for a pushrod. Without a pushrod the actuation mechanism can be simpler, lighter and stiffer. Also the internal structure of a particular wing would be minimally disturbed.

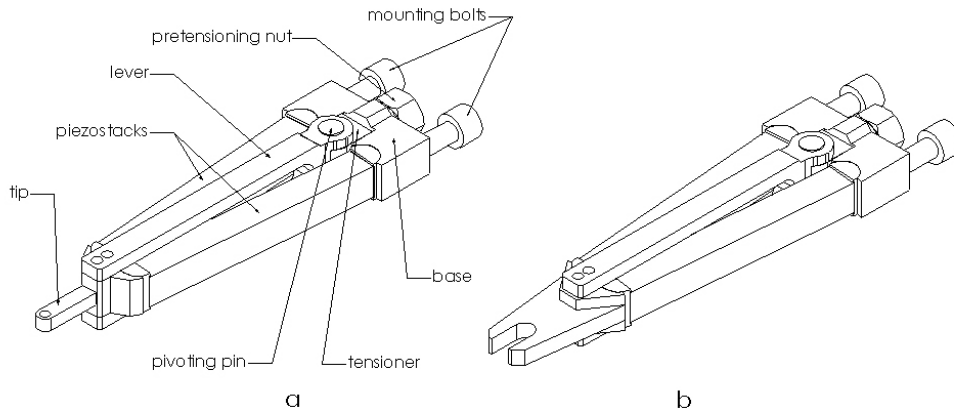


Figure 1: Comparison between the initial design of the actuator, a, and the design for integration into a wing, b.

In the process of finding the best way to integrate the actuator into a wing model, the design of the actuator suffered small changes. Figure 1 shows comparatively the initial design of the actuator and the actuator modified for flap actuation. By using the initial design (Fig. 1a), one could connect the tip of the actuator with the flap through a floating link (for the case of chordwise position of the actuator), or a pushrod (for spanwise position of the actuator). At first, the floating link mechanism seemed to be a good solution. Design analysis conducted using SolidWorks revealed that a crank-slider-like mechanism would be a better solution than the floating link. As a result, the design of the actuator tip was modified in order to accommodate a slider (Figure 1b).

Figure 2 presents a cross-section view of the design of the actuator integration into a wing model. The actuator is attached to the structure through the support, 2, designed such that it will mount on existing elements of the structure. Two bolts are used to secure the actuator in place. For sophisticated constructions one would use an adjustable support in order to place the actuator in the desired position (chordwise and spanwise). Flap actuation is realized as the tip of the actuator moves up and down pushing the slider, 4. There is a close fit between the actuator tip and the slider in order to avoid undesirable nonlinearities (freeplay). The slider is mounted on a pin which is supported on two ball bearings mounted in a support, 6. This support can slide along a slot machined in the flap

rib, 7, and this permits the distance, r_β , between the flap hinge and slider pivot axis to be adjusted at the desired value, as flap deflection is given by

$$\beta = s/r_\beta \quad (1)$$

As the tip of the actuator moves up and down, it pushes the slider causing the flap to rotate about the hinge line. The flap is mounted on ball bearings, for minimal friction losses. In order to minimize friction between the slider and the actuator tip, the slider is made of bronze while the actuator tip is made of high strength steel.

Figure 3 shows pictures of the actual wing model. The internal structure is made of aluminum, balsa wood and steel. The cover (skin) is made of aluminum sheet having a thickness of 0.01 inches.

The wing model was designed and constructed to fit vertically in the wind tunnel at Duke University. The vertical position was chosen in order to eliminate the effect of gravity. The wing was mounted on an existing test rig that permits the two degrees of freedom, plunge and pitch. The rig consists of two mounts that are placed outside the wind tunnel (top and bottom), each being connected to a rigid base through two bands of spring steel that provide the stiffness of the wing in plunge. Two bearings, one in each mount, allow the wing model to be simply supported (hinged) on the mounts at the 1/4 chord by using two pins. Pitch stiffness is provided by a simply supported steel wire which runs through a hole in the upper mounting pin.

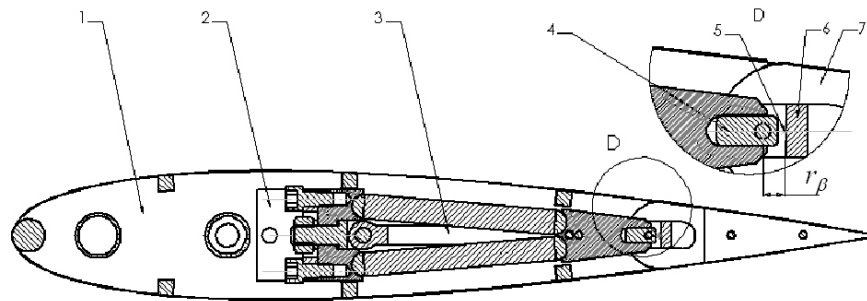


Figure 2: Actuator integration into the wing (SolidWorks model); 1 - wing body, 2 - actuator support, 3 - V-Stack Piezoelectric Actuator, 4 - slider, 5 - flap hinge line, 6 - adjustable support, 7 - trailing edge control surface (flap)

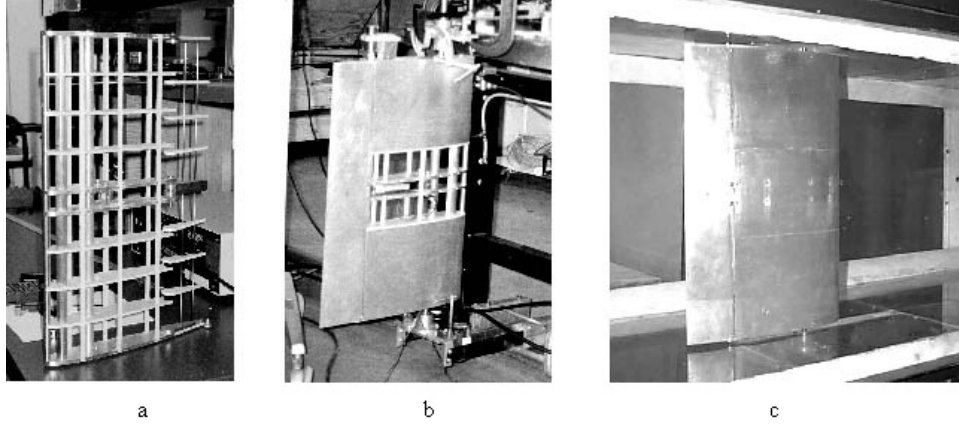


Figure 3: Wing model; a - shows the internal structure; b - wing and test rig on the bench; c - wing model in the wind tunnel

Aerodynamic model of the typical-section wing model

To predict the flutter flow speed and frequency, aerodynamic analysis of the wing model was performed. The analysis method is based on simple beam analysis for structures and unsteady vortex lattice method for aerodynamics.⁷ In the unsteady vortex lattice method, vortices are distributed on the wing as well as in the wake. Various conditions on the vortex strengths are then imposed to solve the problem dynamically. The discrete unsteady vortex lattice relations are summarized below:

- a. Vorticity-downwash relation relates the downwash at the control points on the wing due to structural deflections to the downwash induced by bound and wake vorticity.

$$K_b \Gamma_b^{\frac{n+1}{2}} + K_w \Gamma_w^{\frac{n+1}{2}} - w^{\frac{n+1}{2}} = 0 \quad (2)$$

where, Γ_b and Γ_w denote the strengths of bound and wake vortices, K_b and K_w are the corresponding induced velocity coefficients, w denotes the downwash due to structural deflections, and the superscript denotes the time iteration at which the variable are calculated.

- b. Shed vorticity - bound vorticity relation relates the change in bound vorticity to the wake vor-

ticity shed in that time interval.

$$\sum \Gamma_b^n - \sum \Gamma_b^{n+1} - \Gamma_w^{n+1} = 0 \quad (3)$$

- c. Convection of shed vorticity relation states that at each iteration the vorticity travel at the airspeed to the next vortex element.

$$\Gamma_b^{n+1} - \Gamma_b^n = 0 \quad (4)$$

The equations given above form a complete set of equations representing the dynamics of bound and wake vorticity. The equations are in discrete time, and were derived from continuous time form using finite difference equations. The continuous wake dynamic system of equations is:

$$\{\dot{\Gamma}\} = [A_1]\{\Gamma\} + [A_2]\{W\} \quad (5)$$

where, $[A_1]$ and $[A_2]$ are coefficient matrices which relate the vorticity to structural deformations $\{W\}$. The vector $\{W\}$ can be written in terms of the structural displacement variables.

The aerodynamic equations can be coupled with the structural equations to form a complete aeroelastic model. The structural equations as derived using the beam mode shapes are given by:

$$[M]\{\ddot{q}\} + [K]\{q\} = \{Q\} \quad (6)$$

$[M]$, and $[K]$ are the mass and stiffness matrices, $\{q\}$ are the modal displacements, and, $\{Q\}$ are the

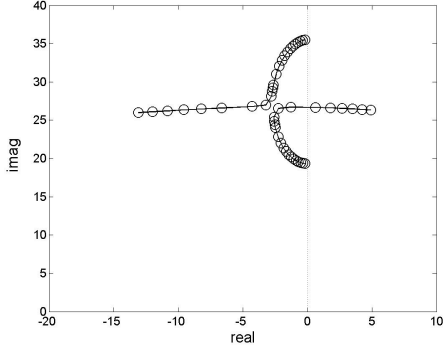


Figure 4: Root locus plot, showing the migration of the poles of the aeroelastic system

modal forces. The modal forces are calculated from the aerodynamic lift distribution. The lift distribution is given by:

$$L = \rho U \Gamma_b + \rho \int_{-b}^x \dot{\Gamma} dx \quad (7)$$

Equations (5) and (6) form a set of linear aeroelastic equations, which are used for predicting the linear response and stability of a wing in airflow. Using the above equations, the model predicted the flutter flow speed at 19 m/s and the flutter frequency at 4.2 Hz. These results have proven to be in good agreement with the wind tunnel experiments. Figure 4 shows a root locus plot of the poles of the aeroelastic system as a function of airspeed (from 1 m/s to 24 m/s). The circles in each plot denote increments of 1 m/s. The modal coalescence is clearly seen.

Experimental results

Bench experiments and results

Before the wind tunnel experiments bench tests were performed in order to evaluate the performance of the newly designed flap actuation system and to verify the characteristics of the test rig. To better predict the flutter parameters in the aerodynamic

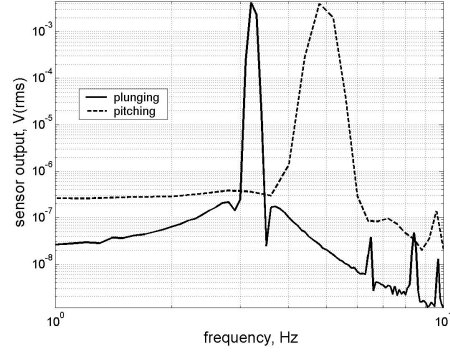


Figure 5: Uncoupled structural natural modes of the experimental rig.

model, the characteristics of the actual experimental rig were used.

The characteristics of the rig (typical-section wing and mounting fixtures) are the following:

Geometrical characteristics

l	=	0.522	m
c	=	0.360	m
b	=	0.180	m
e	=	$-0.5 \times b$	
h_l	=	$0.5 \times b$	
r_β	=	5	mm (adjustable)

Inertial characteristics

CG	=	0.050	m
f_{CG}	=	0.025	m
m	=	2.610	kg
m_w	=	2.258	kg
m_f	=	0.352	kg
m_{bu}	=	0.644	kg
m_{bl}	=	0.392	kg
I_{CG}	=	$2.439 \cdot 10^{-2}$	$\text{kg} \cdot \text{m}^2$
I_{fCG}	=	$2.694 \cdot 10^{-4}$	$\text{kg} \cdot \text{m}^2$

Stiffness characteristics

K_h	=	2341.5	N/m
K_α	=	29.59	$\text{N} \cdot \text{m}/\text{rad}$
K_β	=	15.35	$\text{N} \cdot \text{m}/\text{rad}$

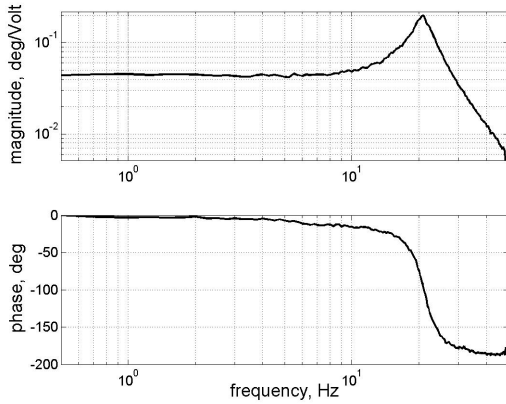


Figure 6: Frequency response plot of the actuator-flap system

Flap hinge stiffness was measured for 75 V DC offset on the actuator piezoelectric stacks; the offset is required when the actuator is in operation. As mentioned above, the test rig allows two degrees of freedom (plunge and pitch) for the wing. The first natural modes for uncoupled case were measured to be 3.2 Hz for plunge and 4.8 Hz for pitch, as shown in Fig. 5, an autospectrum of the sensor signal (rms) measured for transient vibration of the rig in pitch and plunge.

The bandwidth of the actuator-flap system must be above 4.8 Hz in order to be useful for flutter control. Figure 6 shows a first natural mode of the flap at 21 Hz and a bandwidth exceeding 10 Hz. Figure 7 shows a maximum flap deflection of about $\pm 5.5^\circ$. Notice also the hysteretic behavior of the actuator-flap system which is consistent with the actuator hysteretic behavior. Because there are additional losses in the actuation mechanism in addition to those inherent to the actuator, the hysteretic losses for the composite actuator-flap system are greater than those of the actuator itself.

Wind tunnel experiments. Flutter control

For the wind tunnel experiments, the wing was placed vertically inside the wind tunnel, as seen in

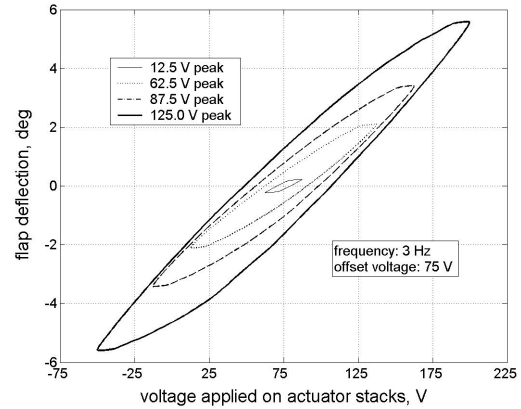


Figure 7: Hysteretic behavior of the actuator-flap system

Fig. 3c, and aligned with the flow (zero angle of attack). The first objective was to determine the actual flutter flow speed. To this end, we recorded time responses of the wing in plunging and calculated damping coefficient using logarithmic decrement.⁸ Figure 8 shows open-loop and closed-loop results. The flow speed at which the damping goes to zero is the flutter speed. For the open-loop wing the flutter speed was determined to be 21.5 m/s, 12% higher than predicted by our numerical aeroelastic model. The numerical model did not include structural damping and we expect this would account for a flutter speed higher than predicted. As the flow speed approaches the flutter speed there is a dramatic change in damping clearly shown in Fig. 8 (see also Fig. 4).

The objective of the closed-loop control test was to stabilize the wing at the open-loop flutter condition, using the trailing edge flap, delaying the onset of flutter until a higher flow speed. Deflecting the flap induces aerodynamic forces and moments that can be used to damp pitching and plunging motions of the wing. Since the aerodynamics, wing structure, and controller are elements of a single dynamic system, it is possible to control flutter by feeding back some measure of the current state of the system, in this case pitch.



Figure 8: Damping factor, ζ , versus flow speed

Figure 9 shows the schematic of the closed-loop control architecture. The controller commands a flap deflection based on a measurement of the current pitching of the wing. To effectively track the commanded flap deflection at the 4 Hz flutter frequency, a continuous-time proportional-integral (PI) servo-controller was designed with proportional gain $K_p = 1.5 \times 10^{-4}$, and integral gain $K_i = 150$. A notch filter was placed in series with the PI controller to compensate for the 21 Hz resonance of the actuator/flap system (see the plant frequency response in Fig. 6). The controller was implemented

on a dSPACE digital control board at a sample rate of 500 Hz. Using the bilinear (Tustin) transformation, the continuous-time controller and notch filter transfer functions were converted to the following discrete-time transfer functions :

$$\text{PI}(z) = \frac{0.00015z + 0.2999}{z - 1} \quad (8)$$

$$\text{notch}(z) = \frac{0.8015z^2 - 1.489z + 0.748}{z^2 - 1.487z + 0.5513} \quad (9)$$

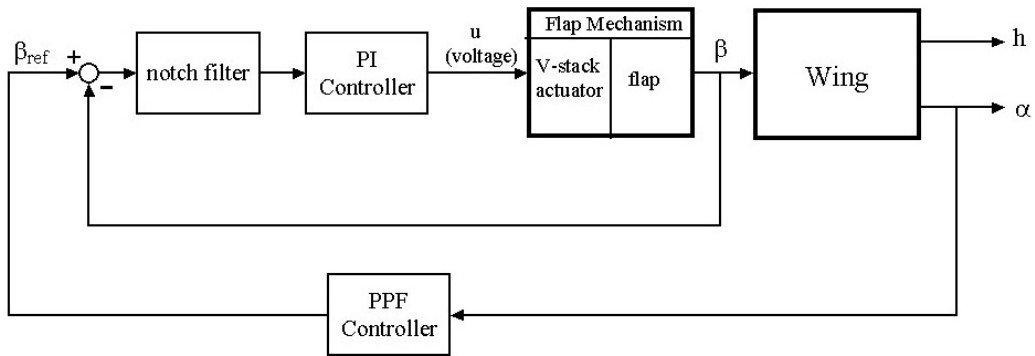


Figure 9: Flutter control schematic

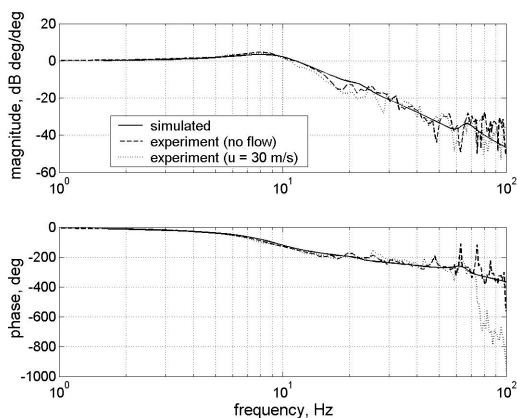


Figure 10: Closed-loop frequency response of servo-controlled flap deflection, β/β_{ref}

Figure 10 shows the simulated and actual experimental frequency response of the flap deflection at no flow and 30 m/s flow (with the wing locked down at pitch and plunge). The flap servo-control system effectively tracks up to 10 Hz regardless of flow conditions.

Positive Position Feedback (PPF) control is used to add damping to the unstable flutter mode. This control approach consists of feeding back a structural displacement through a second-order filter.⁹ This technique is analogous to the tuned-mass vibration absorber. For controller design, a model was measured relating the reference flap deflection to pitch, and its frequency response is shown in Fig.11. The final filter design had a natural frequency of 4.1 Hz, damping coefficient of 0.1, and DC gain of 21, and is represented by the discrete-time transfer function

$$PPF(z) = \frac{-0.01386z^2 - 0.02771z - 0.01386}{z^2 - 1.987z + 0.9898} \quad (10)$$

The control strategy has proven effective for flutter suppression at the flutter speed. When only the flap servo-control was active, the wing experienced limit cycle oscillations in both pitch and plunge, observed for the first 2.8 s in Fig. 12. When the PPF controller was turned on at 2.8 s, the wing motions were significantly reduced. Further closed-loop tests were conducted at increasing flow velocities. Figure

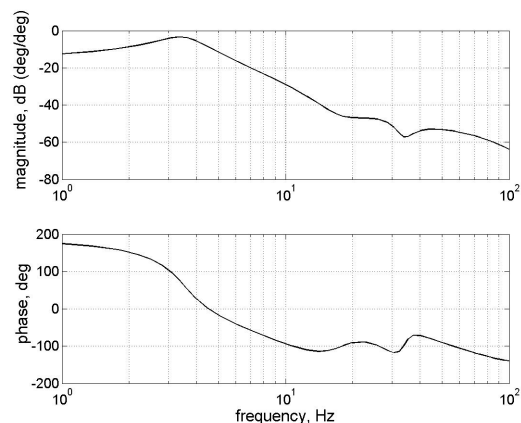


Figure 11: Open-loop frequency response of commanded flap deflection, β_{ref} to measured pitching motion, α

8 shows damping as a function of flow speed. The closed-loop flutter speed is 26.2 m/s, an increase by 21.8% over the open-loop flutter speed. This indicates good performance of the actuation system, thus even further increase in flutter speed is possible upon implementing a MIMO control system that will feed back both pitch and plunge simultaneously.

Summary

A typical-section wing model with integrated V-Stack Piezoelectric Actuator was built and tested on the bench and in the wind tunnel. Experimental results indicate that the scheme of flap actuation is feasible and flutter suppression possible.

The actuator produces the desired flap deflection and the response of the flap (angle of deflection), with respect to the voltage applied across the piezoelectric stacks, exhibits desired linearity, and the actuator-flap system exhibits a bandwidth in excess of 10 Hz.

The flap was servo-controlled using a PI controller and the wing was stabilized above its flutter speed using PPF control. The closed loop flutter speed was 26.2 m/s, an 21.8% increase over the open-loop flutter speed.

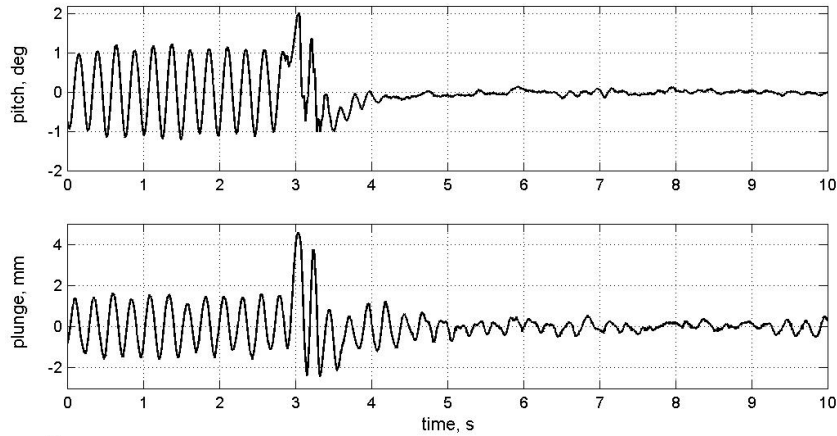


Figure 12: Flutter suppression ($U = 21.5$ m/s). PPF controller turned on at 2.8 s.

Acknowledgements

This work was supported by DARPA through AF-SOR Grant F49620-99-1-00253, Aeroelastic Leveraging and Control Through Adaptive Structures, under the direction of Dr. Ephraim Garcia and Dr. Dan Segalman. We would also like to thank Dr. Earl Dowell, Dr. Deman Tang, and Dr. Mayuresh Patil (Widener University, Chester, PA) for sharing their expertise in aeroelasticity. Thanks to our colleagues in the Adaptive Systems and Structures Laboratory: Dr. Robert Richard, Dr. Jonathan Kemp, Min Moon and Matthew Kozlowski, for useful discussions and assistance. Thanks to senior machinist John Goodfellow for his effort and commitment in machining the parts.

References

- [1] Precht, E. F. and Hall, S. R., “An X-Frame Servo-Flap Actuation System for Rotor Control,” *Proceedings of SPIE Vol. 3329*, pp 309–320, San Diego, CA, March 1998.
- [2] Hall, S. R. and Precht, E. F., “Preliminary Testing of a Mach-Scaled Active Rotor Blade with a Trailing Edge Servo-Flap,” *SPIE Smart Structures and Materials Symposium*, Newport Beach, CA, March 1999.
- [3] Chandra, R. and Chopra, I., “Actuation of Trailing Edge Flap in a Wing Model Using Piezostack Device,” *Journal of Intelligent Material Systems and Structures*, Vol. 9, October 1998, pp. 874–853.
- [4] Koratkar, N. A. and Chopra, I., “Analysis and Testing of Mach-Scaled Rotor with Trailing-Edge Flaps,” *AIAA*, Vol. 38, No. 7, July 2000, pp. 1113–1124.
- [5] Borglund, D. and Kutteneuler, J., “Active Wing Flutter Suppression Using a Trailing Edge Flap,” *Journal of Fluids and Structures*, Vol. 16, No. 3, 2002, pp. 271–294.
- [6] Ardelean, E. V. and Clark, R. L., “V-Stack Piezoelectric Actuator,” *SPIE Smart Structures and Materials*, Vol. 4333, 2001, pp. 322–333.
- [7] Hall, K. C., “Eigenanalysis of Unsteady Flows About Airfoils, Cascades, and Wings,” *AIAA Journal*, Vol. 32, No. 12, December 1994, pp. 2426–2432.
- [8] Thomson, W. T., *Theory of Vibration with Applications*, Prentice-Hall, Inc., Englewood Cliffs, NJ, 1972.
- [9] Fanson, J. and Caughey, T., “Positive Position Feedback Control for Large Space Structures,” *AIAA Journal*, Vol. 28, No. 4, 1990, pp. 717–724.